

XMM-Newton Observations of PSR B1706-44

K.E. McGowan¹, S. Zane², M. Cropper², J.A. Kennea³, F.A. Córdova³, C. Ho¹,
T. Sasseen⁴, W.T. Vestrand¹

mcgowan@lanl.gov

ABSTRACT

We report on the *XMM-Newton* observations of the young, 102 ms pulsar PSR B1706-44. We have found that both a blackbody plus power-law and a magnetized atmospheric model plus power-law provide an excellent fit to the EPIC spectra. The two scenarios are therefore indistinguishable on a statistical basis, although we are inclined to prefer the latter on physical grounds. In this case, assuming a source distance of ~ 2.3 kpc, the size of the region responsible for the thermal emission is $R \approx 13$ km, compatible with the surface of a neutron star. A comparison of the surface temperature of PSR B1706-44 obtained from this fit with cooling curves favor a medium mass neutron star with $M \sim 1.45M_{\odot}$ or $M \sim 1.59M_{\odot}$, depending on two different models of proton superfluidity in the interior. The large collecting area of *XMM-Newton* allows us to resolve a substructure in the broad soft X-ray modulation detected by *Chandra*, revealing the presence of two separate peaks with pulsed fractions of $7 \pm 4\%$ and $15 \pm 3\%$, respectively.

Subject headings: pulsars: individual (PSR B1706-44) — stars: neutron — X-rays: stars

1. INTRODUCTION

PSR B1706-44 is a young ($\tau = 1.7 \times 10^4$ yr), energetic 102 ms pulsar originally discovered by Johnston et al. (1992). It is one of several sources with spin down ages 10^4 – 10^5 yrs which

¹Los Alamos National Laboratory, MS D436, Los Alamos, NM 87545

²Mullard Space Science Laboratory, University College of London, UK

³University of California, Riverside, CA 92521

⁴University of California, Santa Barbara, CA 93106

are referred to as Vela-like pulsars, due to their similar emission properties (Becker & Pavlov 2002). The source is known to display glitches (Johnston & Manchester 1995) and is plausibly associated with the supernova remnant G343.1-2.3 (McAdam et al. 1993; Dodson & Golap 2002; Bock & Gvaramadze 2002).

According to the new Cordes & Lazio (2002) model, the pulsar is ~ 2.3 kpc away, which agrees with the kinematic distance in the range 2.4–3.2 kpc inferred from H I absorption (Koribalski et al. 1995). VLA images (Frail et al. 1994, Giacani et al. 2001) indicated that the pulsar is located inside a synchrotron plerionic nebula about $3''.5 \times 2''.5$ in size. Evidence for a more extended X-ray compact nebula (with radius $\sim 20'' - 30''$) was also found in *ROSAT*-HRI and *Chandra* images (Finley et al. 1998, Dodson & Golap 2002).

PSR B1706-44 is one of only eight radio pulsars which are known to emit in the GeV range (Thompson et al. 1992), and one of only three detected in the TeV range, although this detection is marginal (Kifune et al. 1995, Chadwick et al. 1998). Thompson et al. (1992) found pulsations at the radio period in the *EGRET*-CGRO data. The light curve above 400 MeV is complex, with evidence of two, possibly three peaks, none of which are in phase with the radio peak. We note that the light curve of Vela in the gamma-ray range shows two peaks (Kanbach et al. 1994), and at least three in the X-rays (Strickman et al. 1999; Pavlov et al. 2000). Particular characteristics of the Vela-like pulsars, with respect to the Crab-like pulsars, are that the pulse profiles at different energies are shifted in phase with respect to each other.

An unpulsed X-ray source at the radio-pulsar position had been detected with *ROSAT*-PSPC (Becker et al. 1995), ASCA (Finley et al. 1998) and BeppoSax (Mineo et al. 2002). More recently, deeper *Chandra* observations have been presented by Gotthelf, Halpern & Dodson (2002). These authors discovered a broad sinusoidal X-ray pulsation at the radio-period, with a pulsed fraction of $23\% \pm 6\%$. The phasing of the radio pulse was consistent with that of the center of the broad X-ray peak. The high spectral and spatial resolution of *Chandra* allowed a multi-component fit of the X-ray spectrum revealing the presence of a thermal component: the X-ray spectrum was found to be well-fit with a two component model, with a blackbody temperature of $T = (1.66^{+0.17}_{-0.15}) \times 10^6$ K and a power law index of $\Gamma = 2.0 \pm 0.5$. The blackbody radius $R = 3.6 \pm 0.9$ km determined from the model parameters, suggests that the emission is from a hot spot, or that a fit with an atmospheric model is required (Gotthelf et al. 2002). Hydrogen atmospheres are in general harder than a blackbody since free-free absorption dominates in the X-ray band. Therefore, the temperature fitted by a hydrogen atmosphere is lower than that resulting from a blackbody fit (hence the former fit yields a larger radius).

In this paper we report on *XMM-Newton* observations of PSR B1706-44. Results from

the spectral and timing analyses are presented in the following sections.

2. OBSERVATIONS

PSR B1706-44 was observed with *XMM-Newton* for ~ 40 ks on 2002 March 12, and ~ 46 ks on 2002 March 13, as a part of the Guaranteed Time program. The following analysis uses data from the three European Photon Imaging Camera (EPIC) instruments: two EPIC MOS detectors (Turner et al. 2001) and the EPIC PN detector (Struder et al. 2001). The thin optical blocking filter was used on the PN. To minimize pile-up the PN was operated in *small window* mode, which gives a temporal resolution of 6 ms. The MOS1 was operated in *full window* (imaging) mode with a time resolution of 1.4 s. In order to obtain better temporal resolution the MOS2 was operated in *timing mode*; in this mode data from the central CCD are collapsed into a one-dimensional row to achieve a 1.5 ms time resolution. The medium filter was used for both MOS observations. Observations of PSR B1706-44 were taken with the Resolution Grating Spectrometer (RGS), however we did not detect enough photons for a meaningful analysis. Due to an optically bright source in the field the blocking filter was used on the Optical Monitor (OM).

We reduced the EPIC data with the *XMM-Newton* Science Analysis System (SAS v5.4.1). To maximize the signal-to-noise we filtered the data to include only single, double, triple and quadruple photon events for MOS, and only single and double photon events for PN. We also filtered the events files to exclude times of high background.

PSR B1706-44 is known to be surrounded by a pulsar wind nebula (Gotthelf et al. 2002; Dodson & Golap 2002). In an ideal situation analysis of the source should be carried out on data which are not contaminated by the diffuse emission. However, the nebula is very compact, with the diffuse emission visible between $1''$ and $10'' - 20''$ (see Gotthelf et al. 2002). Therefore the spatial resolution of *XMM-Newton* is not high enough to be able to separate the pulsar from its putative synchrotron nebula. In order to quantify this effect, we have compared PSR B1706-44's emission with that for a point source. We simulated the expected PN data for a point source with similar column depth and spectral characteristics as PSR B1706-44 using *SciSim**. The radial profiles for PSR B1706-44 from 2002 March 12 and 13, and the simulated source, are shown in Fig. 1. The background has been subtracted from both the PSR B1706-44 and point source data. We have normalized the total point source counts to the total counts from PSR B1706-44 by performing a χ^2 minimization to determine the appropriate scaling factor required to fit only the core of the pulsar ($< 5''$).

*<http://xmm.vilspa.esa.es/>

Our results show marginal evidence for an excess of diffuse emission between $5''$ and $20''$. An extraction radius of $< 5''$ does not give a sufficient number of photons for analysis purposes, hence, we have chosen an extraction radius of $20''$. We note that this radius will therefore include emission from the pulsar wind nebula. As only $\sim 75\%$ of the energy from the source is encircled in this radius the measured fluxes have been corrected in the following analyses.

3. SPECTRAL ANALYSIS

Spectra for PSR B1706-44 were extracted from both the PN and MOS1 data, and regrouped by requiring at least 30 counts per spectral bin. We subtracted a background which was extracted from an annulus around the source fiducial region. The corresponding photon redistribution matrix (RMF) and ancillary region file (ARF) were created.

We simultaneously fit the four spectra, two from the PN and two from MOS1, with thermal and power-law models, modified by photoelectric absorption. Results are shown in Fig. 2 and the best-fit parameters are summarized in Table 1. The column density was first fixed at the value given in Gotthelf et al. (2002), $N_H = 5.5 \times 10^{21} \text{ cm}^{-2}$, for the single blackbody, single power-law and blackbody plus power-law fits. As this value was not very well constrained in Gotthelf et al. (2002), we also allowed N_H to vary for the above model fits. We find that the data are poorly fit with a single blackbody for free and fixed N_H , and with a single power-law with fixed N_H . The single power-law model with free N_H fits the data reasonably well, however the two-component blackbody plus power-law model with either free or fixed N_H gives a better fit. We find the two-component fit where the column density is allowed to vary results in $N_H = (4.5_{-0.4}^{+0.7}) \times 10^{21} \text{ cm}^{-2}$, with a temperature $T^\infty = (2.01_{-0.20}^{+0.18}) \times 10^6 \text{ K}$, power-law index $\Gamma = 1.49_{-0.08}^{+0.09}$, and $\chi^2_\nu = 0.84$ for 658 d.o.f. The X-ray luminosity is $1.0 \times 10^{33} \text{ ergs s}^{-1}$ in the $0.2 - 10 \text{ keV}$ band, and the blackbody contribution is $3.8 \times 10^{32} \text{ ergs s}^{-1}$. The distance to PSR B1706-44 is uncertain, with values in the range $1.8 - 3.2 \text{ kpc}$ (Taylor & Cordes 1993; Koribalski et al. 1995). By adopting the value determined from the Cordes & Lazio (2002) free-electron model of the Galaxy, $D = 2.3 \pm 0.3 \text{ kpc}$, we obtain an emitting radius $R^\infty = 1.81_{-0.29}^{+0.43} \text{ km}$, too small to be compatible with a neutron star equation of state. The results for the column density, temperature and power-law index are in good agreement with those obtained by Gotthelf et al. (2002) based on *Chandra* data. While the radius we determine is smaller than that from the fits to the *Chandra* data, Gotthelf et al. (2002) also found that the radius of the emitting region inferred from the blackbody fit of the thermal component indicates a hot region on a cooler surface.

In order to try a more physical description of the thermal component, we fitted the data with a neutron star hydrogen atmosphere plus power-law model. The magnetic field of PSR B1706-44, as inferred from the spin-down rate, is 3×10^{12} G, high enough to have a substantial effect on the opacities (Pavlov et al. 1992; Zavlin et al. 1996; Zane et al. 2000). We used a grid of pure-H, atmospheric cooling models computed for $B = 10^{12}$ G and different effective temperatures, provided by V. Zavlin (V.E. Zavlin 2003, private communication).

We first fixed the neutron star mass and radius at $M_{NS} = 1.4M_{\odot}$, $R_{NS} = 10$ km; all other parameters were allowed to vary. The resulting best-fit parameters are $\Gamma = 1.45^{+0.14}_{-0.01}$, $N_H = (5.2 \pm 0.1) \times 10^{21} \text{ cm}^{-2}$ and $T_{eff} = (1.03^{+0.07}_{-0.31}) \times 10^6$ K, where T_{eff} is the effective temperature evaluated at the star surface (see Table 1). This gives a temperature at infinity $T^{\infty} = (0.79^{+0.07}_{-0.31}) \times 10^6$ K. The source distance resulting from this fit is $D = 1.7 \pm 0.3$ kpc, lower than that computed by Cordes & Lazio (2002). The reliability of the pulsar distance derived using the dispersion measure method is uncertain, however, the distance issue can only be firmly addressed by parallax measurements, which are not available for PSR B1706-44. We therefore fit the data assuming a distance to the source of 2.3 ± 0.3 kpc. By fixing $R_{NS} = 12$ km and repeating the atmospheric plus power-law model fit we find $\Gamma = 1.43^{+0.20}_{-0.05}$, $N_H = (5.1^{+0.2}_{-0.1}) \times 10^{21} \text{ cm}^{-2}$ and $T_{eff} = (1.01^{+0.01}_{-0.34}) \times 10^6$ K [$T^{\infty} = (0.82^{+0.01}_{-0.34}) \times 10^6$ K]. The distance to the pulsar from this fit is $D = 2.1 \pm 0.2$ kpc, in agreement with the value obtained from the dispersion measure.

Due to the goodness of fit for both the blackbody plus power-law, and the magnetic atmosphere plus power-law models we are unable to distinguish between these two scenarios on only a statistical basis. Taken at face value, these results indicate that the emission is either from the whole neutron star surface with radius ~ 12 km, or that the thermal X-rays originate from a smaller region, i.e. a hot spot.

4. TIMING ANALYSIS

For the timing analysis the event files were filtered on energy, to include only photons in the range 0.2 – 10 keV. The filtered event files were then barycentrically corrected. We extracted data for the PN from a circular region centered on the source of radius $20''$. Selection of the photons from the MOS2 event files was achieved by extracting 90% of the flux within a rectangular region centered on the source. The fluxes have been corrected for this in the following temporal analysis. To increase the signal-to-noise we have combined the PN data from 2002 March 12 and 13. We also combined the MOS2 datasets.

We determine a predicted pulse period at the epoch of our *XMM-Newton* observations for

PSR B1706-44, assuming a linear spin-down rate and using the radio measurements (Wang et al. 2000; Gotthelf et al. 2002). We find $P = 102.477638$ ms ($f = 9.7582265$ Hz) at the start of our first observation (MJD 52345.0), and $P = 102.477654$ ms ($f = 9.7582249$ Hz) at the end of our second observation (MJD 52347.0). As the frequency of the predicted period varies over the duration of our observations, and glitches and/or deviations from a linear spin-down may alter the period, we searched for a pulsed signal in the PN and MOS2 data over a wider frequency range centered on $f = 9.75823$ Hz.

We have employed two methods in our search for pulsed emission from PSR B1706-44. In both methods we have included the frequency derivative from Gotthelf et al. (2002) in our calculations to determine the best-fit frequency. In the first method we implement the Z_n^2 test (Buccheri et al. 1983), with the number of harmonics n being varied from 1 to 5. In the second method we calculate the Rayleigh Statistic (see de Jager 1991; Mardia 1972) and then calculate the Maximum Likelihood Periodogram (MLP) using the ΔC -statistic (Cash 1979) to determine significant periodicities in the datasets (see Zane et al. 2002).

The most significant Z_n^2 -statistic for the combined PN data occurs for $n = 1$. With the number of harmonics equal to one, the Z_n^2 -statistic corresponds to the well known Rayleigh statistic. We find a peak at $f = 9.7582258_{-0.0000009}^{+0.0000007}$ Hz (see Fig. 3, *top left panel*). The quoted 90% uncertainty range is determined from the error in the position of the peak. Within errors, the peak in the Z_1^2 periodogram lies in the range of predicted frequencies. The Z_1^2 -statistic for this peak is 41.82, which has a probability of chance occurrence of 8.3×10^{-10} . The corresponding peak in the MLP periodogram occurs at $f = 9.7582263_{-0.0000005}^{+0.0000001}$ Hz (Fig. 3, *bottom left panel*). Within the 90% confidence limit, this value is consistent with the predicted radio frequency, and the frequency found from the Z_1^2 periodogram.

We generated Z_n^2 and MLP periodograms for the MOS2 data as for the PN data. There is a peak at $f = 9.7582258$ Hz in the Z_1^2 and MLP periodograms, however it is not the most significant peak. There are several peaks present in both periodograms, the significance of which are low compared to the noise level. The individual PN datasets from 2002 March 12 and 13 have $S/N = 5.0$ and $S/N = 6.5$, respectively. The MOS2 data from the same dates both have $S/N = 1.6$. The low signal-to-noise ratio of the MOS2 data is the cause for the lack of a significant peak at the predicted frequency.

5. FOLDED LIGHT CURVE

As our *XMM-Newton* observations were taken more than a year outside the valid range of the radio ephemeris given in Gotthelf et al. (2002) we are unable to determine a phase

relationship between the X-ray and radio pulse profiles. Hence, we have used an arbitrary ephemeris $T_0 = \text{MJD } 52346.2$. We folded the PN and MOS2 data on the frequency found from the Z_1^2 periodogram, $f = 9.7582258$ Hz. The effects of the drifting period are taken into account by including the frequency derivative in the calculations.

In Fig. 4 we show the combined PN, MOS2 and PN plus MOS2 pulse profiles. We modeled the folded light curves with one and two sinusoids; the resulting χ_ν^2 values are given in Table 2. As it can be seen, the fits to the data are improved with the double sinusoidal model. To determine the statistical significance of the second sinusoid we employed an F-test. We find F-test probabilities of 9×10^{-5} , 3×10^{-3} and 4×10^{-5} , for the PN, MOS2 and PN plus MOS2 fits respectively. These values indicate that the PN and PN plus MOS2 data are best-fit with the two sinusoid model, while no firm conclusion can be derived from the low S/N MOS2 data. The pulsed fractions of the two peaks are $7 \pm 4\%$ and $15 \pm 3\%$.

In an attempt to investigate if the two peaks in the folded light curve are thermal or non-thermal in origin, we determined from the two-component model fits to the spectra the energy at which the power-law starts to dominate over the thermal emission. This occurs at ~ 1.23 keV, and ~ 1.34 keV in the blackbody plus power-law and magnetic atmosphere plus power-law models, respectively. By filtering the PN and MOS2 event files on energy we produced light curves in the following energy ranges $0.2 - 1.35$ and $1.35 - 10.0$ keV, which we barycentrically corrected. We folded the data on $f = 9.7582258$ Hz (Fig. 5), again including the frequency derivative in the calculations. As we can see, the same features are present in both bands; the thermal and non-thermal emission are both pulsating and phase aligned. However, at higher energies the modulation is lower, indicating that the power law component is contaminated by the non-pulsating nebular emission.

6. DISCUSSION

6.1. Spectral Results

Of the > 1000 radio pulsars detected so far, only $< 5\%$ have also been found in the X-rays. These X-ray emitting pulsars represent a wide range of ages ($10^3 - 7 \times 10^9$ yrs), magnetic field strengths ($10^8 - 10^{13}$ G), periods ($1.6 - 530$ ms) and spectral properties. In particular, only a sub-set of them are suitable for observing the thermal radiation from the neutron star surface, and therefore constrain the atmospheric chemical composition and the pulsar cooling history. Thermal emission from the neutron star surface is not detectable in pulsars older than 10^6 yr: standard cooling scenarios predict a sharp reduction in the surface temperature when surface photon emission overtakes the neutrino luminosity losses

(Nomoto & Tsuruta 1987). In pulsars younger than 10^4 yr strong non-thermal emission from the magnetosphere or the synchrotron nebula swamps the weaker thermal radiation and dominates the X-ray spectrum. Only in middle-aged pulsars (ages $10^4 - 10^6$ yr), is the non-thermal component much fainter; hence for such objects the thermal radiation from the neutron star surface ($T \sim 0.02 - 0.1$ keV) can dominate at soft X-ray/UV energies.

To date, thermal emission has been detected in only very few radio pulsars, e.g. PSR B0656+14 (Possenti et al. 1996), PSR B1055-52 (Pavlov et al. 2002), PSR J0437-4715 (Zavlin et al. 2002), PSR J0538+2817 (McGowan et al. 2003), Geminga (Halpern & Wang 1997), Vela (Pavlov et al. 2001), and PSR B1706-44 (Gotthelf et al. 2002). The thermal emission detected above ~ 0.5 keV in the spectrum of the first four objects has been more plausibly interpreted as originating from a hot-polar cap. This agrees with the fact that these older sources should have a surface flux peaked in the UV and it is confirmed by a detection, in the brightest PSR B0656+14, of a further thermal component below 0.7 keV (Pavlov et al. 2002). The younger Vela pulsar ($\tau = P/2\dot{P} \sim 10^4$ yr) is the only radio active source for which the thermal component observed in the soft X-rays is well explained by a magnetized cooling atmosphere (Pavlov et al. 2001). When this model is assumed instead of a blackbody, the inferred radius increases from $R^\infty/d_{294} \approx 2.5$ km to $R^\infty/d_{294} \approx 15^{+6.5}_{-5.1}$ km (where d_{294} is the distance in units of 294 pc) and is therefore in agreement with a standard neutron star equation of state. The only other neutron stars whose thermal component is better described by an atmospheric model, and for which this interpretation resolves all the inconsistencies which follow from the blackbody interpretation, are the radio-silent neutron stars 1E 1207-52 (Zavlin et al. 1998) and RX J0822-4300 (Zavlin et al. 1999).

Here we present a further example. We have found that both a blackbody plus power-law and a magnetized atmospheric model plus power-law provide an excellent fit to the data, and are indistinguishable on a statistical basis. However, the latter has to be preferred on physical grounds, as we argue below, and, at a source distance of 2.3 kpc, gives an emitting area of $R = 13.41^{+1.75}_{-4.84}$ km, compatible with the size of a neutron star (Lattimer & Prakash 2001).

Our knowledge of neutron star interiors is still uncertain and accurate measurements of the neutron star surface temperature are particularly important to constrain the cooling models and provide information on the physics of the neutron star. Roughly speaking, theoretical models predict a two-fold behavior of the cooling curves. In low-mass neutron stars neutrino emission is mainly due to a modified Urca process and nucleon-nucleon bremsstrahlung. These are relatively weak mechanisms and produce *slow cooling*. In stars of higher mass the neutrino emission is enhanced by a direct Urca process (or other mechanisms in exotic matter), therefore these stars cool down much faster (*fast cooling* regime). To date (see Yakovlev

et al. 2002 for a recent a discussion) it has been realized that simple models which do not account for proton and neutron superfluidity fail in explaining the surface temperatures observed in many sources, unless objects such as e.g. Vela, Geminga, RX J1856-3754 do have exactly the critical mass that bounds the transition between the very different *slow cooling* and *fast cooling* regimes. This unlikely assumption can be avoided by including the effects of nucleon superfluidity. Models with proton superfluidity included predict an intermediate region between fast cooling and slow cooling curves, which is expected to be populated by medium mass neutron stars (roughly with M between 1.4 and 1.65 M_{\odot}). Although the full picture only holds if, at the same time, neutron superfluidity is assumed to be rather weak, it is still interesting that many neutron stars (as 1E 1207-52, Vela, RX J1856-3754, PSR 0656+14) have a surface temperature which falls in such a transition region. Since the cooling curves in the transition region show a significant spread with the neutron star mass, if this scenario is correct we can select those curves which explain the observations and therefore attribute certain masses to the sources (“weighing” neutron stars, Kaminker et al. 2001). As we can see from the first two panels of Figure 2 in Yakovlev et al. (2002), assuming an age of $\log \tau = 4.23$, the surface temperature of PSR B1706-44 derived from the blackbody fit is even higher than the upper cooling curves i.e. those corresponding to the slow cooling regime. However, the surface temperature $\log T^{\infty} = 5.9$ obtained by fitting with the magnetized model and $R = 12$ km falls well within the above mentioned transition region of medium mass neutron stars. The mass of PSR B1706-44 should then be $\sim 1.45 M_{\odot}$ or $\sim 1.59 M_{\odot}$, depending on the kind of proton superfluidity assumed in the model (1p and 2p respectively). We note that interpreting the temperatures obtained from the spectral fits in the context of theoretical cooling curves relies on the true age of the pulsar being the same as the characteristic spin-down age, which may not be valid.

6.2. Timing Results

The first detection of pulsations in the soft X-rays of PSR B1706-44 by *Chandra* was a broad modulation in the light curve, approximately in phase with the radio peak (Johnston et al. 1992; Gotthelf et al. 2002). It is known that the radio and gamma-ray pulses are not aligned, with the gamma-ray emission occurring ~ 0.37 cycles after the radio emission (Thompson et al. 1996). The *XMM-Newton* data allows us to resolve the substructure of the soft X-ray light curve, revealing the presence of two separate peaks. However, due to the lack of a contemporaneous radio observation of this glitching pulsar, we are unable to determine an absolute phase relationship between the X-ray, radio and gamma-ray pulse profiles.

To investigate the origin of the pulsed emission in PSR B1706-44 it is instructive to

consider the timing behavior of Vela, since both sources have similar spectral properties. The complex multiwavelength light curves of Vela are the subject of continued interest and some evidence of correlations between the different energy bands have recently been established (Harding et al. 2002). Unfortunately, in the case of Vela, the key to deciphering pulsar emission mechanisms was the light curve in the 2 – 30 keV *RXTE* energy band (obtained with a 92 ks and a ~ 300 ks pointing, Harding et al. 2002), while a 132 ks *RXTE* observation of PSR B1706-44 only gave an upper limit on the pulsed emission in the 9 – 18 keV band (Ray et al. 1999).

The pulse profile of Vela obtained with *EGRET* shows two distinct narrow pulses, at phase ~ 0.1 and ~ 0.55 , neither aligned with respect to the radio peak. Considerable emission has been detected in the phase interval between the peaks (Kanbach et al. 1994). By contrast, in the *EGRET* band PSR B1706-44 shows a broader modulation that extends over the full range of phases between $\sim 0.2 - 0.6$, and is likely to consist of two broad peaks separated by ~ 0.2 (Thompson et al. 1996). No gamma-ray emission is detected outside of the peaks and, as in Vela, the *EGRET* pulses are out of phase with respect to the radio pulse. The difference in the gamma-ray light curves of the two sources is likely to be indicative of a different beaming geometry, with PSR B1706-44 having greater alignment between the rotational and magnetic axes. This is also confirmed by radio-polarization studies (Guojun et al. 1995). An alternative, but indistinguishable scenario is in terms of different viewing angles, in which case PSR B1706-44 should be viewed more equator-on than Vela.

The soft X-ray profile of Vela obtained with *Chandra* shows at least three peaks (Pavlov et al. 2000), at phases $\approx 0.1, 0.4, 0.8$. The presence of several different pulses may be explained in terms of non-thermal radiation originating from more than one region in the pulsar magnetosphere (the soft X-ray pulse profile has a total pulsed fraction of $\sim 8\%$). However, only the first two peaks have a plausible association with *EGRET* (and *RXTE*, see Harding et al. 2002) peaks at similar phases. Although this association is more conclusive for the first peak, if it is the case, this suggests that the emission is probably caused by non-thermal radiation. On the other hand, radiation emergent from a stellar atmosphere is inherently anisotropic regardless of the local temperature and magnetic field, and, when combined with a non-uniform temperature profile at the neutron star surface, is capable of generating considerable pulsar modulation. Also, pulsations are expected if the thermal flux originates from hot polar caps. In this respect, the fact that the third soft X-ray peak does not have a counterpart in the gamma-rays led to speculation that it may be thermal in origin (Pavlov et al. 2000).

In these *XMM-Newton* observations of PSR B1706-44 we have found evidence for two peaks in the soft X-rays. Whether there are similarities between these peaks and those in the

soft X-ray light curve of Vela, and the underlying emitting scenario, is unclear. We find that for PSR B1706-44 the overall X-ray pulsation is much more prominent at softer energies, below ~ 1 keV, but unfortunately a comparison between the light curves in different energy bands does not allow us to establish unequivocally the thermal or non-thermal character of the two peaks (see Fig. 5). In fact, due to the modest spatial resolution of *XMM-Newton*, the power-law component detected in the X-ray spectrum is probably highly contaminated by the non-pulsating nebula, which explains the overall decrease of the pulsed fraction at higher energies. However, we do observe the modulation in both bands and there is not a significant energy-dependent change in the phasing.

As mentioned above, it has been only recently that deep multiwavelength observations of Vela have successfully proven that the source has nearly phase-aligned pulse profiles and a spectral continuity from X-rays to gamma-rays (Harding et al. 2002). This is of great importance, since the connection between the pulse profiles in different bands was not proven before in Vela-like pulsars, even at a phenomenological level. PSR B1706-44 is considerably weaker than Vela and it lies in the Galactic Center region where the diffuse gamma and X-ray radiation is more intense. However, our results indicate that the soft X-ray pulse profile of PSR B1706-44 consists of two peaks, which may be similar to the Vela light curve in the soft X-ray energies. To determine if PSR B1706-44 is in fact “Vela-like” not only spectrally, but also temporally, future spectrally resolved X-ray observations with high throughput in the 2 – 30 keV band, with contemporaneous radio observations, are required.

7. ACKNOWLEDGMENTS

We thank the anonymous referee for helpful comments. We are grateful to V.E. Zavlin for providing a grid of magnetized cooling atmosphere models. The authors thank Gavin Ramsey and Sergey Trudolyubov for discussions on timing issues. This work is based on observations obtained with *XMM-Newton*, an ESA science mission with instruments and contributions directly funded by ESA Member States and NASA. The authors acknowledge support from the Institute of Geophysics and Planetary Physics (IGPP) program at LANL and NASA grants S-13776-G and NAG5-7714.

REFERENCES

- Becker, W., Brazier, K.T.S., & Trümper, J., 1995, A&A, 298, 528
- Becker, W., & Pavlov, G., 2002, (astro-ph/0208356)

- Bock, D.C.-J., & Gvaramadze, V.V., 2002, A&A, 394, 533
- Buccheri, R., Bennett, K., Bignami, G.F., et al., 1983, A&A, 128, 245
- Cash, W., 1979, ApJ, 228, 939
- Chadwick, P.M., Dickinson, M.R., Dipper, N.A., et al., 1998, APh, 9, 131
- Cordes, J.M., & Lazio, T.J.W., 2002, (astro-ph/0207156)
- de Jager, O.C., 1991, ApJ, 378, 286
- Dodson, R., & Golap, K., 2002, MNRAS, 334, 1
- Finley, J.P., Srinivasan, R., Yoshitaka, S., et al., 1998, ApJ, 493, 884
- Frail, D.A., Goss, W.M., & Whiteoak, J.B.Z., 1994, ApJ, 437, 781
- Giacani, E.B., Frail, D.A., Goss, W.M., & Vieytes, M., 2001, AJ, 121, 3133
- Gotthelf, E.V., Halpern, J.P., & Dodson, R., 2002, ApJ, 567, 125
- Guojun, Q., Manchester, R.N., Lyne, A.G., et al., 1995, MNRAS, 274, 572
- Halpern, J.P., & Wang, F.Y-H., 1997, ApJ, 477, 905
- Harding, A.K., Strickman, M.S., Gwinn, C., et al., 2002, ApJ, 576, 376
- Johnston, S., Lyne, A.G., Manchester, R.N., et al., 1992, MNRAS, 255, 401
- Johnston, S., Manchester, R.N., Lyne, A.G., et al., 1995, A&A, 293, 795
- Kaminker, A.D., Haensel, P., & Yakovlev, D.G., 2001, A&A, 373, L17
- Kanbach, G., Arzoumanian, Z., Bertsch, D.L., et al., 1994, A&A, 289, 855
- Kifune, T., Tanimori, T., Ogio, S., et al., 1995, A&A, 438, 91
- Koribalski, B., Johnston, S., Weisberg, J.H., & Wilson, W., 1995, ApJ, 441, 756
- Lattimer, J.M., & Prakash, M., 2001, ApJ, 550, 426
- Mardia, K.V., 1972, Statistics of Directional Data (London:Academic)
- McAdam, W.B., Osborne, J.L., & Parkinson, M.L., 1993, Nature, 361, 516
- McGowan, K.E., Kennea, J.A., Zane, S., et al., 2003, ApJ, 591, 380

- Mineo, T., Massaro, E., Cusumano, G., & Becker, W., 2002, A&A, 392, 181
- Nomoto, K., & Tsuruta, S., 1987, ApJ, 312, 711
- Pavlov, G.G., Shibano, Yu.A., & Zavlin, V.E., 1992, MNRAS, 253, 193
- Pavlov, G.G., Sanwal, D., Garmire, G.P., et al., 2000, AAS Meeting 196, #37.04
- Pavlov, G.G., Zavlin, V.E., Sanwal, D., et al., 2001, ApJ, 552, L129
- Pavlov, G.G., Zavlin, V.E., & Sanwal, D., 2002, Proceedings of the 270. WE-Heraeus Seminar on “*Neutron Stars, Pulsars and Supernova Remnants*”, eds. W. Becker, H. Lesh & J. Trümper, p. 273-286
- Possenti, A., Mereghetti, S., & Colpi, M., 1996, A&A, 313, 565
- Ray, A., Harding, A.K., & Strickman, M., 1999, ApJ, 513, 919
- Strickman, M.S., Harding, A.K., & de Jager, O.C., 1999, ApJ, 524, 373
- Strüder, L., Briel, U., Dennerl, K., et al., 2001, A&A, 365, 18
- Taylor, J.H., & Cordes, J.M., 1993, ApJ, 411, 674
- Thompson, D.J., Arzoumanian, Z., Bertsch, D.L., et al., 1992, Nature, 359, 615
- Thompson, D.J., Bailes, M., Bertsch, D.L., et al., 1996, ApJ, 465, 385
- Turner, M.J.L., Abbey, A., Arnaud, M., et al., 2001, A&A, 365, 27
- Wang, N., Manchester, R.N., Pace, R.T., et al., 2000, MNRAS, 317, 843
- Yakovlev, D.G., Gnedin, O.Y., Kaminker, A.D., et al., 2002, (astro-ph/0306143)
- Zane, S., Turolla, R., & Treves, A., 2000, ApJ, 537, 387
- Zane, S., Haberl, F., Cropper, et al., 2002, MNRAS, 344, 345
- Zavlin, V.E., Pavlov, G.G., & Shibano, Yu.A., 1996, A&A, 315, 141
- Zavlin, V.E., Pavlov, G.G., & Trümper, J., 1998, A&A, 331, 821
- Zavlin, V.E., Trümper, J., & Pavlov, G.G., 1999, ApJ, 525, 959
- Zavlin, V.E., Pavlov, G.G., Sanwal, D., Manchester, R.N., Trümper, J., Halpern, J.P., Becker, W., 2002, ApJ, 569, 894

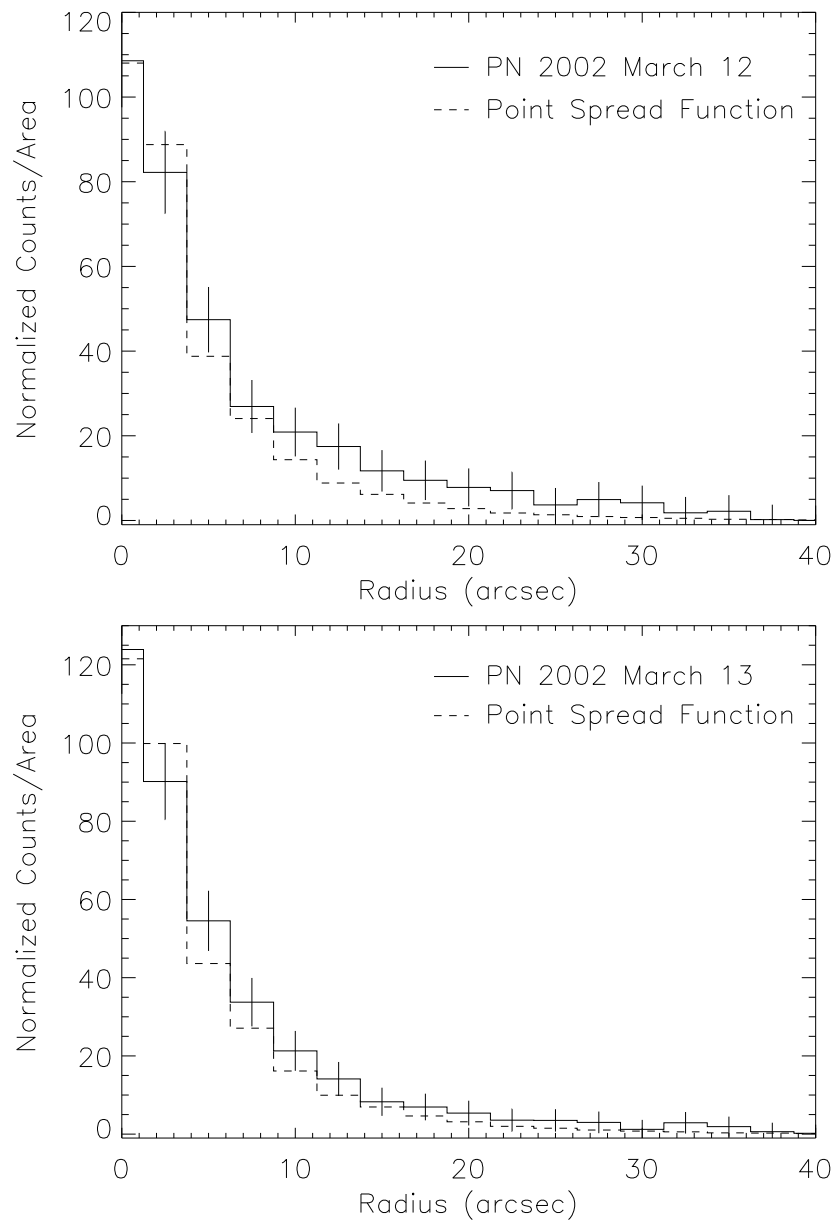


Fig. 1.— X-ray emission from PSR B1706-44 as a function of radius (*solid line*), compared to emission from a simulated point source (*dashed line*; see text). PN observations from 2002 March 12 (*top*) and 13 (*bottom*).

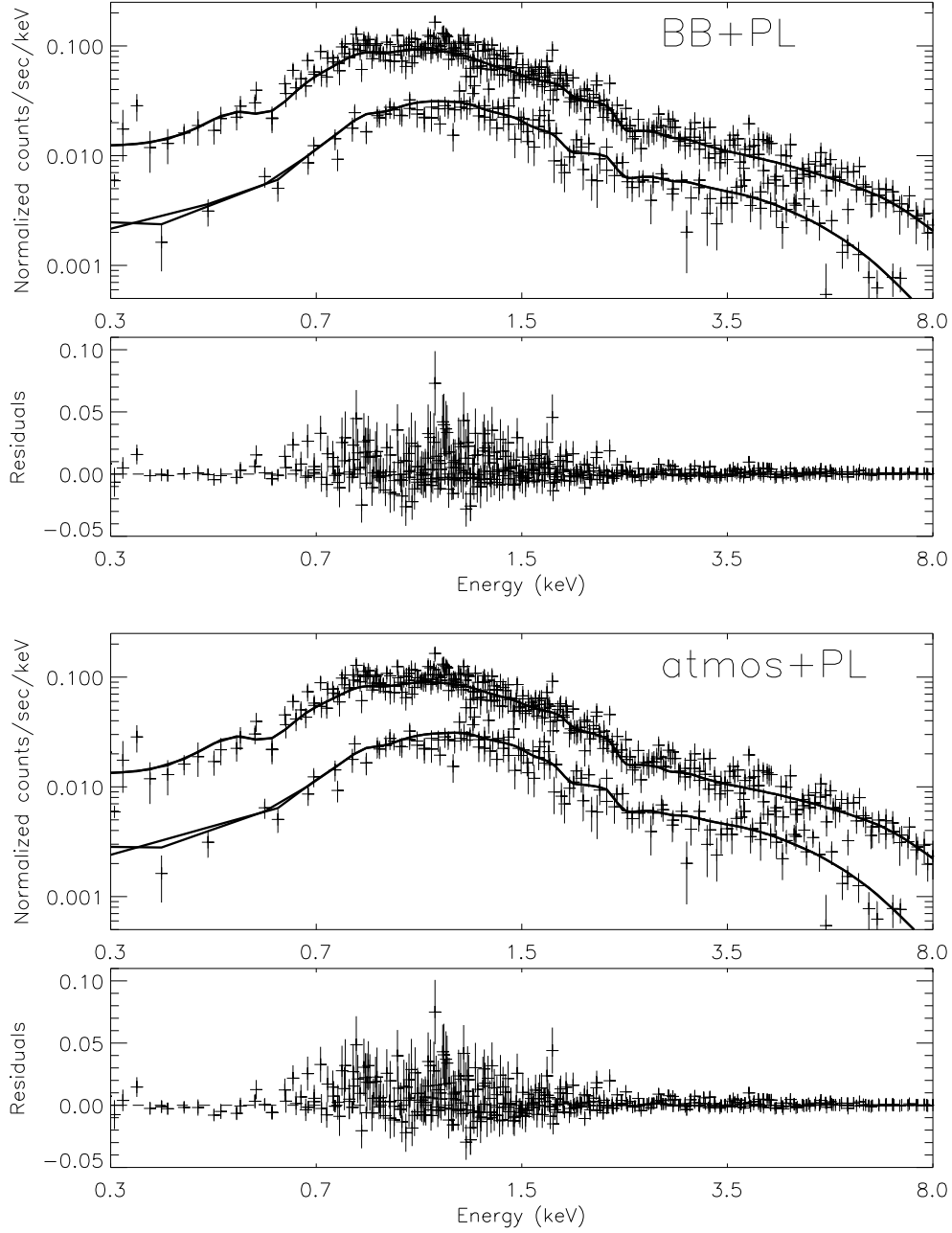


Fig. 2.— PN and MOS1 spectra of PSR B1706-44. First panel, data (*crosses*) and best-fit blackbody plus power-law model with free N_H (*thick line*) for the parameters given in Table 1. Second panel, the difference between the data and the blackbody plus power-law model. Third panel, data (*crosses*) and best-fit magnetic atmosphere plus power-law model (*thick line*) for the parameters given in Table 1, where the radius of the neutron star was fixed at 12 km. Second panel, the difference between the data and the magnetic atmosphere plus power-law model.

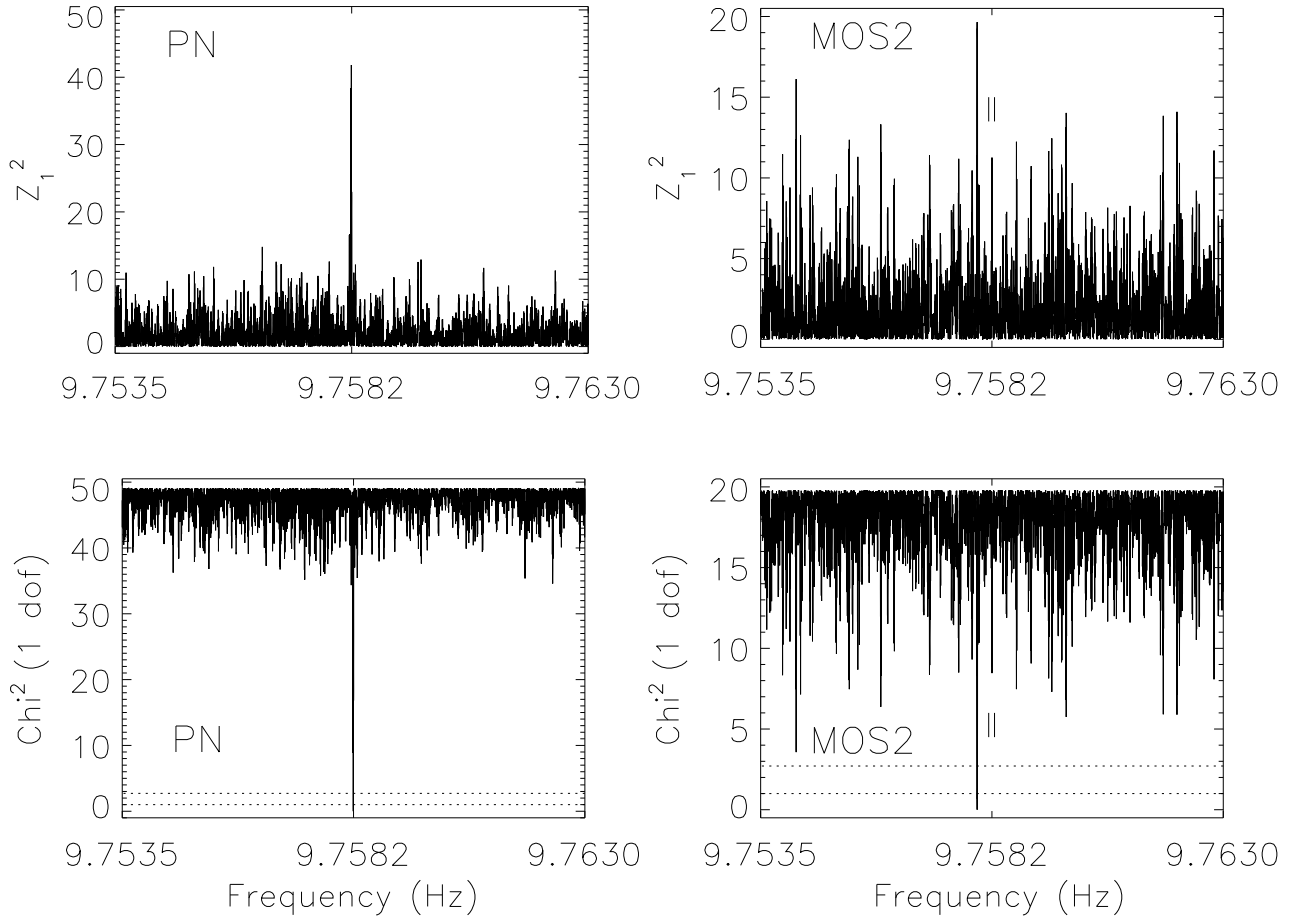


Fig. 3.— Z_1^2 (*top*) and maximum likelihood periodograms (*bottom*) for the combined PN (*left*) and MOS2 data (*right*) of PSR B1706-44. The highest peak in the Z_1^2 periodogram for the PN data occurs at 9.7582258 Hz, with the corresponding MLP peak at 9.7582263 Hz. The peak nearest to the predicted frequency in the MOS2 Z_1^2 periodogram and MLP occurs at $f = 9.7582258$ Hz and is marked by two *solid lines*. The 68% and 90% confidence levels for the periods in the MLP are at $\chi^2 = 1.0$ and 2.71 (*dotted lines*).

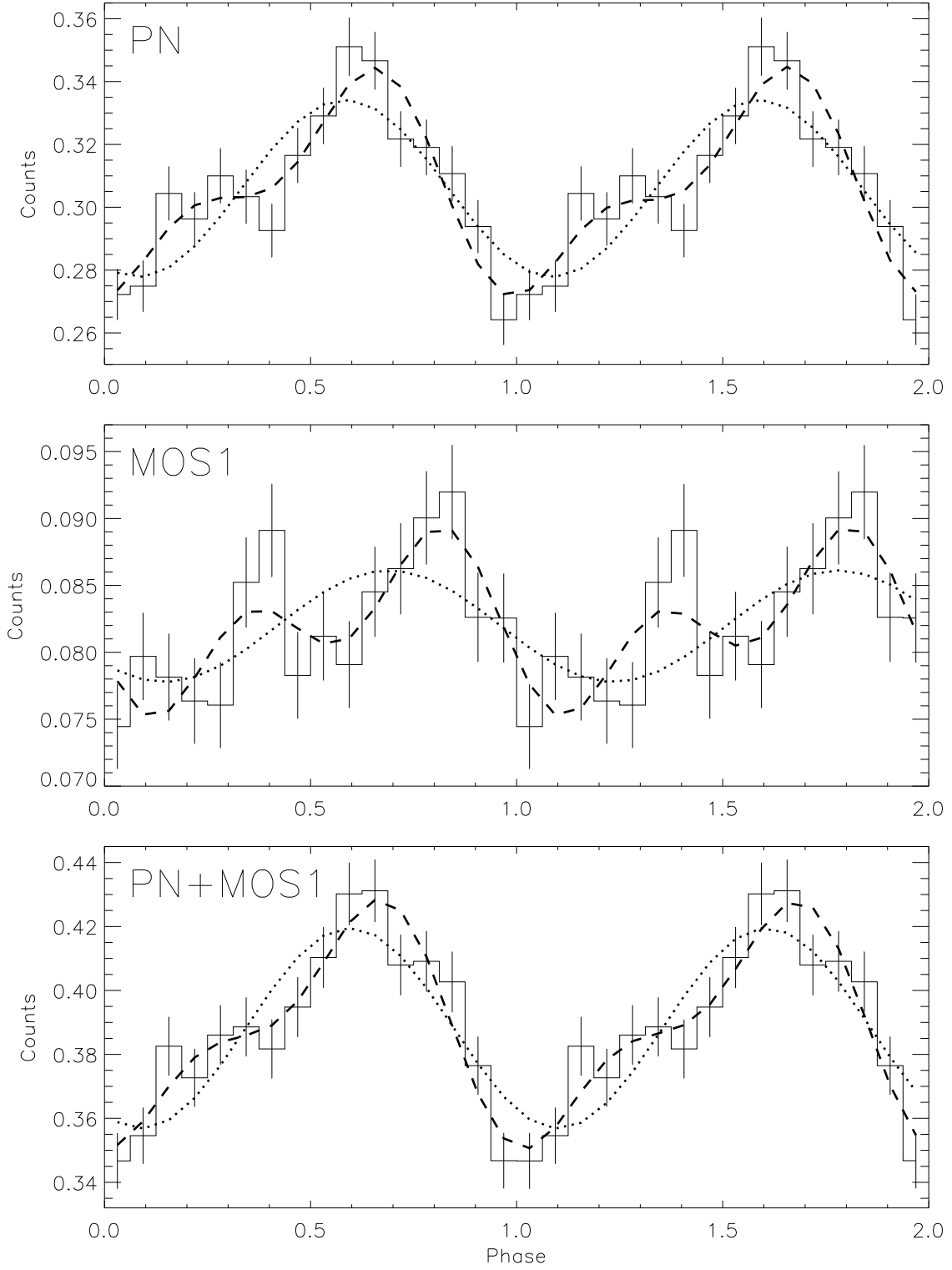


Fig. 4.— Pulse profiles for PSR B1706-44. Data are folded using $f = 9.7582258$ Hz. *Top panel*, combined PN data; *middle panel*, combined MOS2 data; *bottom panel*, combined PN and MOS2 data. Best-fit models are shown, one sinusoid (*dotted line*), two sinusoids (*dashed line*).

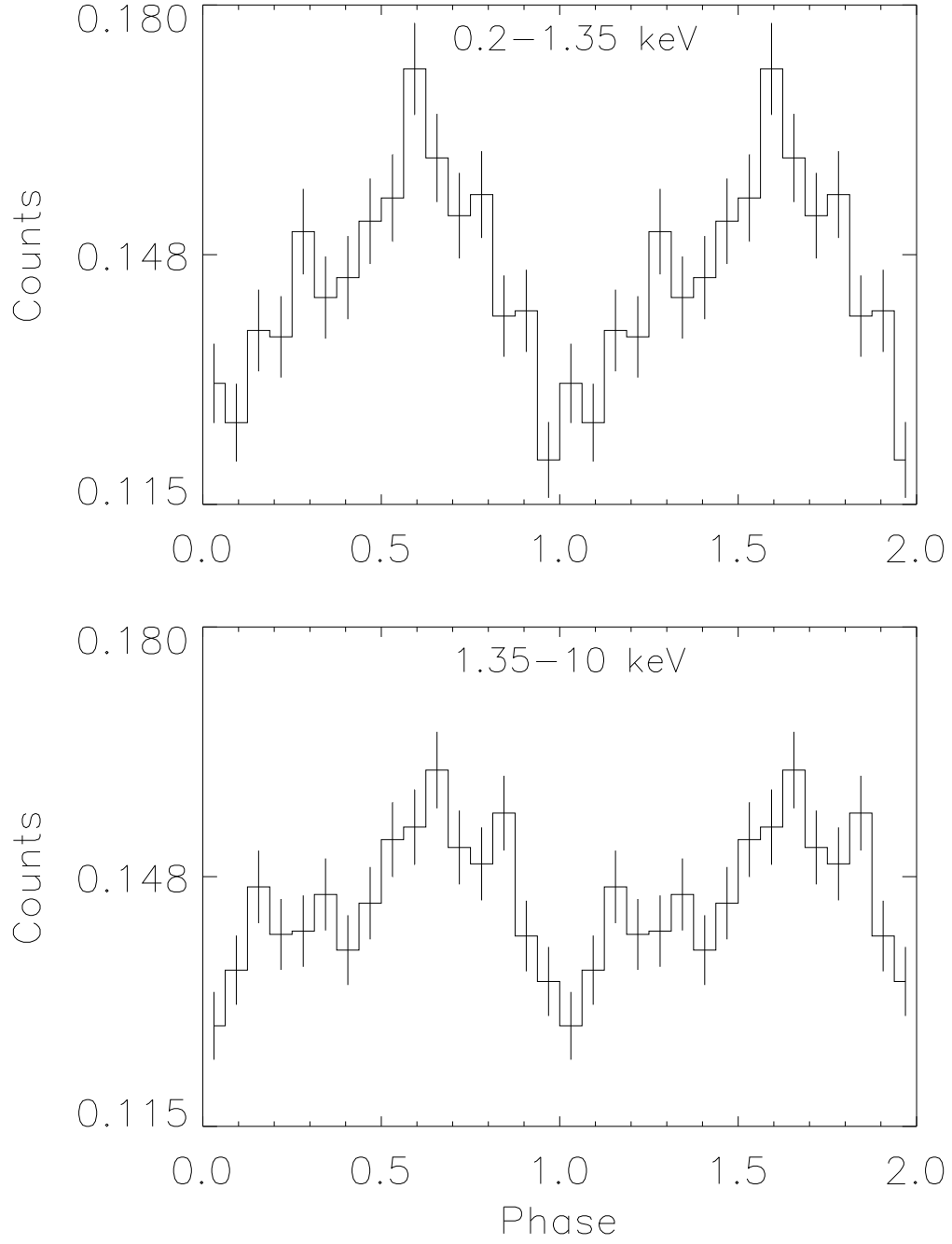


Fig. 5.— Pulse profiles for combined PN and MOS2 data for PSR B1706-44 in different energy ranges. Data are folded using $f = 9.7582258$ Hz. *First panel*, 0.2 – 1.35 keV; *second panel*, 1.35 – 10.0 keV.

Table 1. Spectral fits to PSR B1706-44

Model	N_H $\times 10^{21} \text{ cm}^{-2}$	Γ	R km	T^∞ $\times 10^6 \text{ K}$	D kpc	χ^2_ν [dof]
BB	5.5 (fixed)	\dots	$0.75^{+0.06, a}_{-0.04}$	$3.28^{+0.08}_{-0.12}$	2.3 ± 0.3 (fixed)	4.88 [661]
BB	$0.001^{+0.058}_{-0.001}$	\dots	$0.10^{+0.04, a}_{-0.02}$	$8.14^{+1.14}_{-1.18}$	2.3 ± 0.3 (fixed)	2.92 [660]
PL	5.5 (fixed)	$2.45^{+0.05}_{-0.05}$	\dots	\dots	2.3 ± 0.3 (fixed)	1.82 [661]
PL	$2.9^{+0.2}_{-0.2}$	$1.83^{+0.05}_{-0.05}$	\dots	\dots	2.3 ± 0.3 (fixed)	1.17 [660]
BB+PL	5.5 (fixed)	$1.57^{+0.07}_{-0.06}$	$3.23^{+0.22, a}_{-0.20}$	$1.76^{+0.06}_{-0.06}$	2.3 ± 0.3 (fixed)	0.84 [659]
BB+PL	$4.5^{+0.7}_{-0.4}$	$1.49^{+0.09}_{-0.08}$	$1.81^{+0.43, a}_{-0.29}$	$2.01^{+0.18}_{-0.20}$	2.3 ± 0.3 (fixed)	0.84 [658]
atmos+PL	$5.2^{+0.1}_{-0.1}$	$1.45^{+0.14}_{-0.01}$	10 (fixed)	$0.79^{+0.07}_{-0.31}$	1.7 ± 0.3	0.84 [658]
atmos+PL	$5.1^{+0.2}_{-0.1}$	$1.43^{+0.20}_{-0.05}$	12 (fixed)	$0.82^{+0.01}_{-0.34}$	2.1 ± 0.2	0.84 [658]

Note. — The atmospheric cooling models are computed for $B = 10^{12} \text{ G}$, pure-H chemical composition, and have been provided by V. Zavlin (?). The local temperature T_{eff} obtained from the atmospheric fits have been redshifted to infinity according to $T^\infty = T_{eff} \sqrt{1 - 2GM/Rc^2}$, with R given in the 4th column and $M = 1.4 M_\odot$.

^a Note that this is the value of the radius redshifted at infinity, while the entries in the atmospheric fits are the model parameter R , i.e. the radius measured at the star surface.

Table 2. χ^2_ν values for sinusoidal fits to the PN, MOS2, and PN plus MOS2 data

Data	1 sinusoid χ^2_ν [dof]	2 sinusoids χ^2_ν [dof]
PN	2.6 [28]	1.3 [25]
MOS2	1.7 [28]	1.1 [25]
PN+MOS2	2.0 [28]	0.9 [25]